Available online at www.sciencedirect.com

ScienceDirect

Acta Materialia 77 (2014) 248–257

Acta MATERIALIA

www.elsevier.com/locate/actamat

Cryogenic-temperature-induced transition from shear to dilatational failure in metallic glasses

M.Q. Jiang [a,b,*], G. Wilde [b], J.H. Chen [a], C.B. Qu [c], S.Y. Fu [c], F. Jiang [d], L.H. Dai [a,*]

[a] State Key Laboratory of Nonlinear Mechanics, Institute of Mechanics, Chinese Academy of Sciences, Beijing 100190, People's Republic of China
[b] Institute of Materials Physics, Westfälische Wilhelms-Universität Münster, Münster 48149, Germany
[c] Technical Institute of Physics and Chemistry, Chinese Academy of Sciences, Beijing 100190, People's Republic of China
[d] State Key Laboratory for Mechanical Behavior of Materials, Xi'an Jiaotong University, Xi'an 710049, People's Republic of China

Received 17 March 2014; received in revised form 12 May 2014; accepted 27 May 2014
Available online 1 July 2014

Abstract

At temperatures well below the glass transition temperature, the failure of metallic glasses is generally induced by shear banding, which is a result of the self-organized shear transformation zones (STZs). Here, we demonstrate that, upon cooling down to liquid helium temperature (4.2 K), a Zr-based bulk metallic glass under quasi-static uniaxial tension can fracture via cavitation, rather than by shear banding, showing a transition from shear- to dilatation-dominated failure. This transition is supported by the breakdown of low-temperature strengthening of materials, as well as the changes in the macroscopic failure mode from shear to tension and in the microscopic fracture morphology from vein patterns to fine dimples or nanoscale periodic corrugations. According to the Mohr–Coulomb criterion, it is revealed that the capability of this glass to dilatation is enhanced with decreasing temperature, indicating the temperature-dependent normal stress sensitivity of failure. Our result implies that the shear-dominated STZs will convert into dilatation-dominated operations at very low temperatures.

Keywords: Metallic glass; Shear band; Shear transformation zone; Dilatation; Cryogenic temperature

1. Introduction

Mechanical failure of metallic glasses continues to fascinate researchers [1–5], since dislocations, grain boundaries, crystallographic planes, etc., are not defined in this class of non-crystalline materials [6–9]. Instead, the shear transformation zone (STZ), i.e. the inelastic rearrangement of local atomic groups, is proposed as the fundamental unit of deformation of metallic glasses [10–13]. It is well known that STZs involve both shear and dilatation; in most cases, the former is dominant and the latter is minor. This results in the emergence of 10-nm-scaled shear bands, which macroscopically leads to shear-dominated failure [14,15]. However, recent experiments [14,16–18] and simulations [1,3] have revealed that the dilatation itself, whether induced by shear or hydrostatic tension, can dominate the brittle failure of metallic glasses. In this case, the crack tip propagates via cavitation events that involve a series of nanoscale void nucleation and coalescence processes with very limited plastic growth. The cavitation-mediated brittle failure is strongly suggested by the resulting fracture surface morphologies [14,16–17,19]: very fine dimples that are approximately equiaxed in shape and nanoscale periodic corrugations.

* Corresponding authors. Postal address: State Key Laboratory of Nonlinear Mechanics, Institute of Mechanics, Chinese Academy of Sciences, No 15 Beisihuanxi Road, Beijing 100190, People's Republic of China (M.Q. Jiang). Tel.: +86 10 82543931; fax: +86 10 82543977.
E-mail addresses: mqjiang@imech.ac.cn (M.Q. Jiang), lhdai@lnm.imech.ac.cn (L.H. Dai).

http://dx.doi.org/10.1016/j.actamat.2014.05.052
1359-6454/

It has been well documented that the inherent shear-and-dilatation coupling in STZs leads to the pressure (or normal stress) sensitivity of macroscopic failure (flow and fracture) of metallic glasses [20,21]. Two direct pieces of evidence of such pressure sensitivity are that fracture angles under either compression or tension always deviate from the maximum shear stress plane (45°) [22–24]; and shear stresses at yielding depend on the applied hydrostatic pressure or normal stress [24–26]. Because STZs are stress-driven, thermally activated events initiated around high free-volume regions, it can be seen that the pressure sensitivity depends on the loading mode [23,25] and is highly material/structure specific [25,27–29]. It is expected that temperature could also affect the pressure sensitivity of metallic glass failure, but this needs further experimental evidence.

In this work, we systematically investigated the failure behavior of a typical Zr-based (Vitreloy 1) bulk metallic glass by using environmental temperature as the only controlling parameter. A significant transition from shear to tensile failure was observed by the cryogenic cooling of Vitreloy 1 that was subjected to in situ quasi-static uniaxial tension from room temperature (300 K) to liquid helium temperature (4.2 K). This provides solid evidence that the dilatation of metallic glasses and the resulting normal stress sensitivity of failure are temperature dependent. The observed critical transition phenomenon coincides with the physical picture of the shear-to-dilatation transition in STZs at low temperatures, as originally proposed by Argon [10].

2. Experimental

We chose the Vitreloy 1 bulk metallic glass as the model material because it is a tough system, with room-temperature fracture toughness up to over 80 MPa $\sqrt{m}$ [30], and it has high thermal stability [31]. Vitreloy 1, with a nominal composition of $Zr_{41.2}Ti_{13.8}Cu_{12.5}Ni_{10.0}Be_{22.5}$ (at.%), was cast into plates of dimensions $2 \times 30 \times 60\ mm^3$ in an arc-melter with an in situ suction facility. Dog-bone-shaped specimens with gauge dimensions of $13 \times 2 \times 2\ mm^3$ were

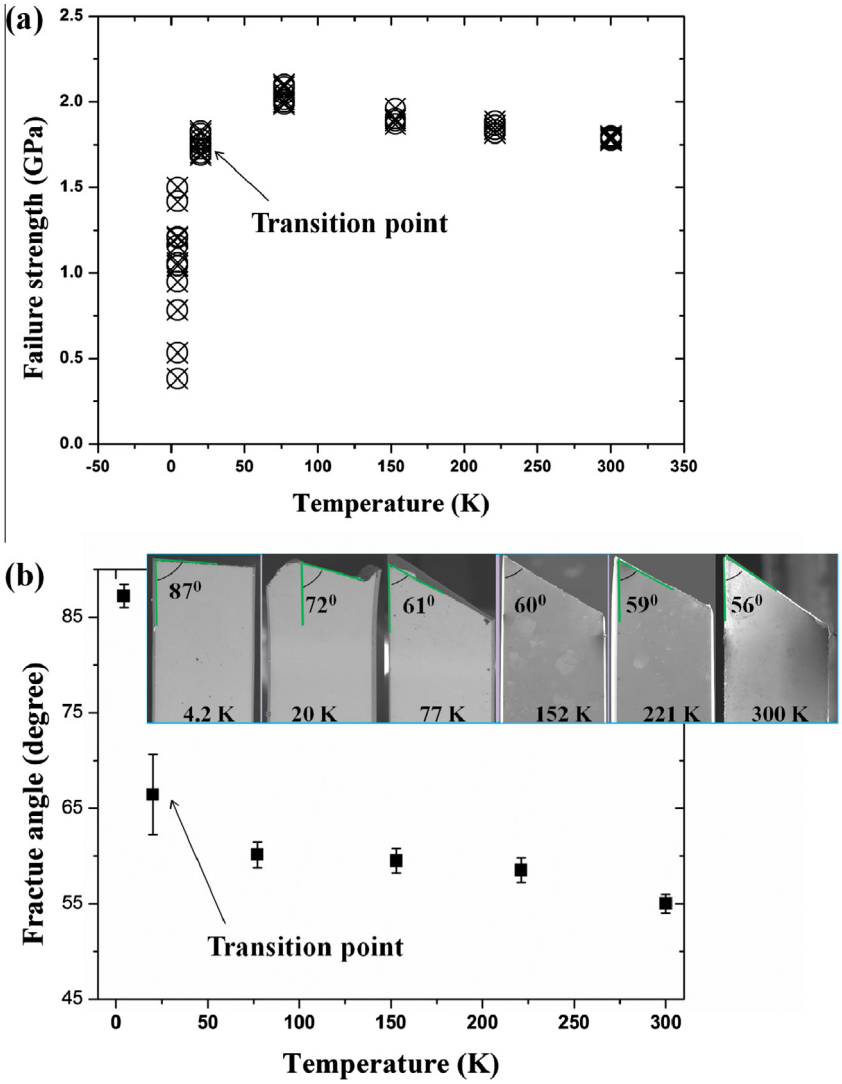

Fig. 1. (a) Tensile failure strength and (b) fracture angle as a function of temperature from room temperature (300 K) down to liquid helium temperature (4.2 K). The inset in (b) shows the representative failure modes at different temperatures.

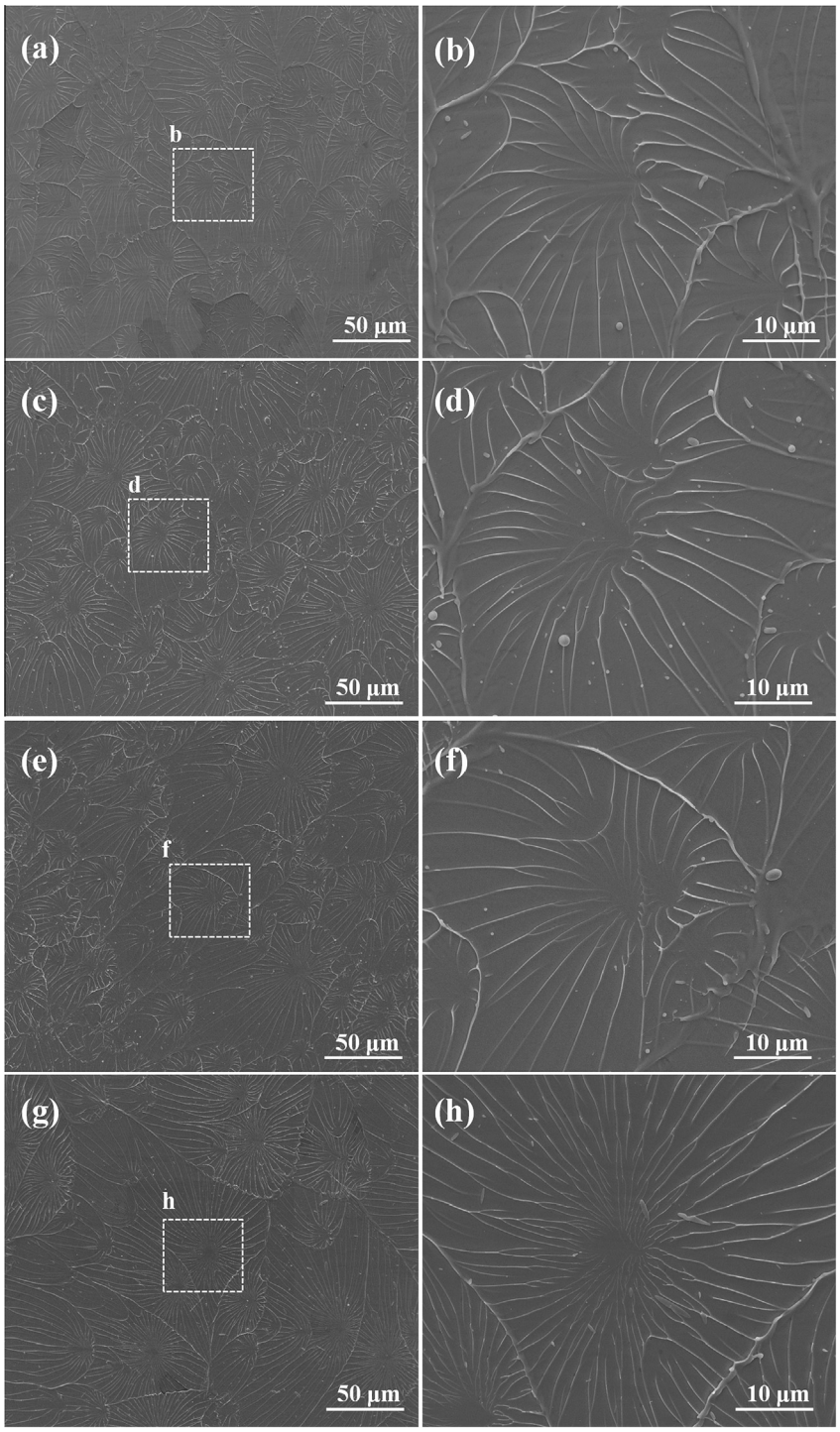

Fig. 2. SEM micrographs of fracture surface morphology in shear failures. (a) 300 K, (c) 221 K, (e) 152 K, (g) 77 K. (b), (d), (f) and (h) are magnified images of the regions within the squares in (a), (c), (e) and (g), respectively.

machined from the as-cast plates and then finely polished. Uniaxial tensile tests were carried out using an Instron material testing machine with an in situ low-temperature environmental facility at a fixed strain rate of $\sim 10^{-4}\ s^{-1}$. Six representative temperatures were adopted: 300, 221, 152, 77, 20 and 4.2 K. At least 10 specimens were tested at each temperature to ensure the reliability of the experimental results. Prior to and during the tension tests, the cryogenic environment was attained and maintained, respectively, by circulating liquid nitrogen or liquid helium through the specimen cabin, and the specimens were cooled to the preset temperatures by controlling the circulation rate of the liquid nitrogen or helium. After testing, fracture surfaces of all specimens were examined in an FEI Sirion scanning electron microscope (SEM) or a 3-D laser scanning confocal microscope.

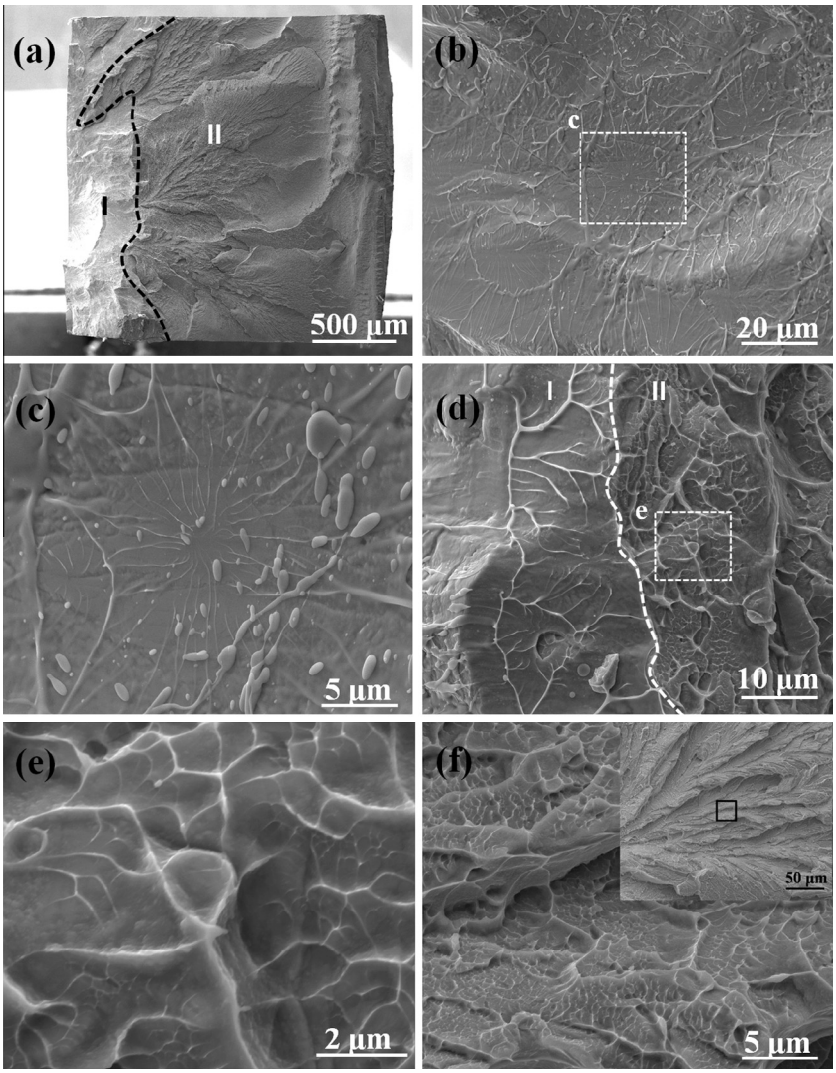

Fig. 3. SEM micrographs of fracture surface at 20 K. (a) Full view of fracture surface, featuring two distinct regions, marked I and II. (b) Vein patterns in region I. (c) A flower-like pattern is observed in area c in (b). (d) A clear boundary between regions I and II. (e) Dimple patterns corresponding to area e in (d). (f) Crack microbranching of the area marked in the inset, which shows the whole feature.

3. Results

3.1. Failure strength

Fig. 1a shows the tensile failure strength σ_f of Vitreloy 1 as a function of the environmental temperature T. The failure strength increases gradually with decreasing temperature from 300 to 77 K, which is consistent with the observations in other Zr-based metallic glasses [32–35]. However, with further decreasing temperature to 20 K, the failure strength is found not to increase any more, but starts to decrease instead. When the materials are cooled down to 4.2 K, their failure strengths decrease further, and scatter across a comparatively wide range, rather than remaining at a constant value. It is well known that discrete failure strengths at a certain temperature usually imply the occurrence of brittle fracture [36]. Similar behavior was reported by Wu and Spaepan [37] in studying the embrittlement of Fe-based metallic glass ribbon, where the constant fracture bending strain became discrete below a critical temperature.

3.2. Failure mode

The fracture angle θ between the loading axis and the fracture plane was measured for all specimens, and the variation of θ with temperature is shown in Fig. 1b. The inset in Fig. 1b presents the macroscopic failure modes at different temperatures. It can be seen that, at temperatures of 300, 221, 152 and 77 K, the fracture angles are about 56°, 59°, 60° and 61°, respectively, falling in the common range for metallic glasses under uniaxial tensions [29,38,39]. This means that the failure in these cases is dominated by shear stress, but is also affected by normal stress. With decreasing temperature, the deviation from 45° becomes larger, implying that the normal stress has a more significant effect on the shear failure. Surprisingly, the fracture plane at 4.2 K is approximately perpendicular to the loading axis,

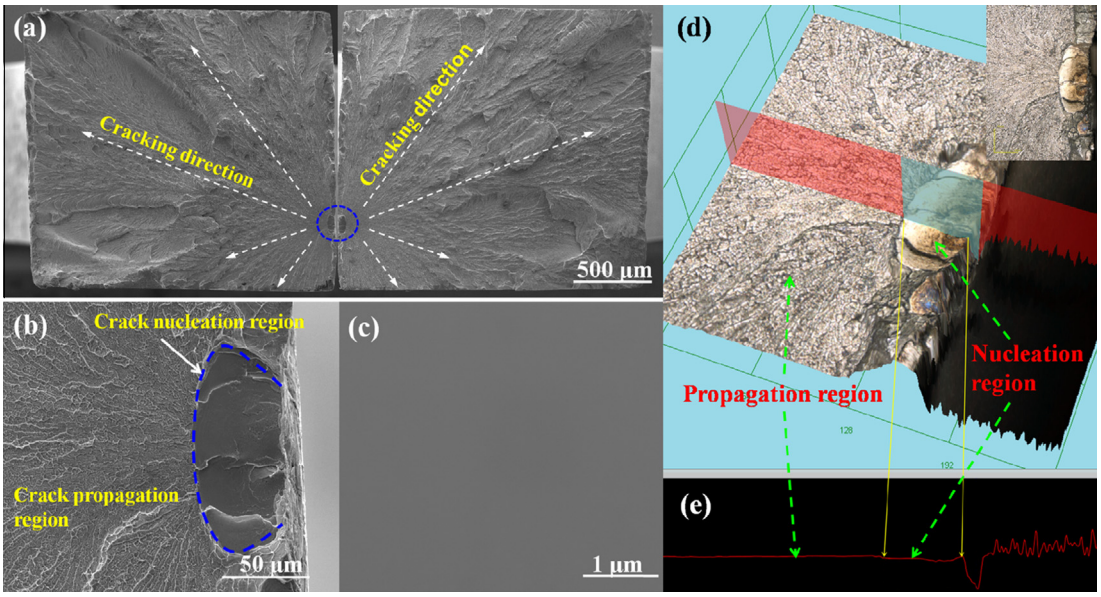

Fig. 4. (a) Matched fracture surfaces of a fractured specimen at 4.2 K, showing a crack nucleation region and a propagation region along the cracking direction. (b) A magnified view of the two regions. (c) A high-resolution SEM observation on the crack nucleation region in (b). (d) A 3-D laser optical micrograph of the crack nucleation and propagation regions. The inset shows the corresponding 2-D micrograph. (e) A surface profile across the two regions.

with a θ of about 87°. This indicates that the failure at 4.2 K is dominated by mode I or tensile cracking rather than by shear banding. At the temperature of 20 K, multiple fracture planes are observed, indicating a mixed failure mode, including both shear and tension. Clearly, the present cryogenic cooling induces a shear-to-tensile transition of failure in Vitreloy 1, and the temperature of about 20 K can be identified as the critical transition point.

3.3. Fracture surface morphology

Fig. 2 shows the fracture surface morphologies at temperatures of 300 K (Fig. 2a and b), 221 K (Fig. 2c and d), 152 K (Fig. 2e and f) and 77 K (Fig. 2g and h). Typical flower-like vein patterns are observed on these fracture surfaces, which has been explained well by the Saffman–Taylor flow instability of the crack front [40,41]. The patterns induced by flow instability strongly suggest that the failures in these temperature cases are triggered by shear. In addition, some smooth cores can be observed on the fracture surfaces. It has been accepted that these smooth cores correspond to local nucleation sites of the crack due to the effect of the normal tensile stress on the fracture planes [23,42–44].

At the transition point (20 K), the fracture surface shows two regions with distinct patterns (marked I and II in Fig. 3a). Region I exhibits the typical vein pattern (see Fig. 3b), with some flower-like patterns (Fig. 3c shows a magnified view of region C in Fig. 3b), as can be seen in the shear failure cases (Fig. 2). Fig. 3d shows the boundary between regions I and II, across which fine dimples (Fig. 3e) and crack microbranches (Fig. 3f) occur, which become the dominant patterns in region II. The vein pattern and the dimple/microbranching coexist on the same fracture surface, further confirming that the specimens at 20 K underwent a mixed shear-and-tensile failure mode (see the inset in Fig. 1b).

The fracture surfaces of the specimens that failed at 4.2 K exhibit a fully brittle fracture feature. Fig. 4a shows the matching fracture surfaces of a fractured specimen. It is evident that the entire fracture surface includes a crack nucleation region and a propagation region along the cracking direction (a magnified view shown in Fig. 4b). High-resolution SEM observation (Fig. 4c) reveals that the nucleation region is very smooth and featureless. Fig. 4d shows a 3-D laser optical micrograph corresponding to Fig. 4b, with the corresponding 2-D image shown in the inset. Fig. 4e presents a surface profile across the crack nucleation and propagation regions, which clearly indicates that the two regions (or the entire fracture surface) are in nearly the same plane. Other fractured specimens at 4.2 K display identical results. These observations provide solid evidence that the crack nucleation region is a nucleated new crack that is formed during fracture rather than a pre-existing surface flaw. Fig. 5 displays the dominant fracture patterns: very fine dimples and nanoscale periodic corrugations are observed in the propagation region. Fig. 5a and b shows the equiaxial dimple patterns at different magnifications, indicating the cavitation mechanism. Fig. 5c and d exhibits a pair of dimple patterns lying in the two matched fracture surfaces (Fig. 4a), clearly showing peak-to-peak and valley-to-valley separation. Fig. 5e and f shows the transition of dimple patterns to nanoscale periodic corrugations. This transition is

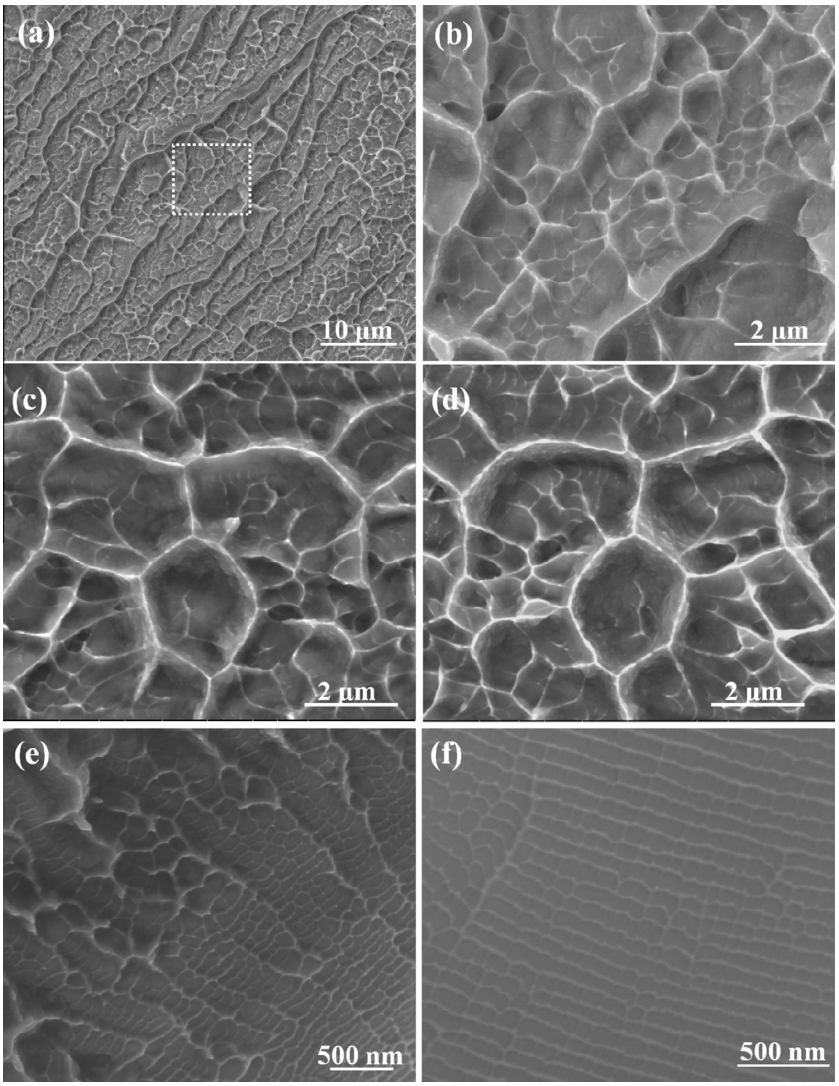

Fig. 5. (a) Typical dimple patterns in the crack propagation region. (f) A magnified view of the marked area in (a). (c and d) A pair of matched dimples on the two fracture surfaces of a fractured specimen. (e and f) The transition of dimples to nanoscale periodic corrugations.

usually due to the acceleration of crack propagation in the final stage [45]. It demonstrates that the two patterns have an identical nature of cavitation, as revealed previously [14,19,46].

3.4. Strength scaling law at 4.2 K

According to classical fracture mechanics [36], brittle fracture of materials is extremely sensitive to the crack nucleation process. This directed us to re-examine the crack nucleation region. We noticed that the nucleation region has two length scales: width W and length L. For the specimen shown in the inset of Fig. 6, $W \approx 50$ μm and $L \approx 117$ μm. We measured the width and length of the nucleation regions of all of the specimens that failed at 4.2 K, and plotted these sizes against the macroscopic failure strengths $\sigma_{f,4.2K}$ in Fig. 6. Very interestingly, the scattered failure strengths show a direct correlation with the length, but are almost insensitive to the characteristic widths, which are nearly constant (about 50 μm). Further analysis uncovers a scaling law between the failure strength $\sigma_{f,4.2K}$ and the characteristic size L of nucleated cracks, which can be expressed by

$$\sigma_{f,4.2K} = K_{I.42K} \cdot \frac{1}{\sqrt{2\pi L}}, \quad (1)$$

where $K_{I,4.2K} \approx 5$ MPa $\sqrt{\text{m}}$ is a fitting parameter. Eq. (1) means that linear elastic fracture mechanics can describe well the tensile failure strength of metallic glasses that is governed by the crack nucleation process corresponding to different degrees of stress concentrations. In this sense, the parameter $K_{I,4.2K}$ can be regarded as the stress intensity factor or fracture toughness [36]. This implies that the temperature decrease from 300 to 4.2 K leads to a significant drop in fracture toughness of Vitreloy 1 of at least one order of magnitude. The estimated fracture toughness of the as-cast Vitreloy 1 at 4.2 K is comparable to the room-temperature value of the heavily annealed Vitreloy

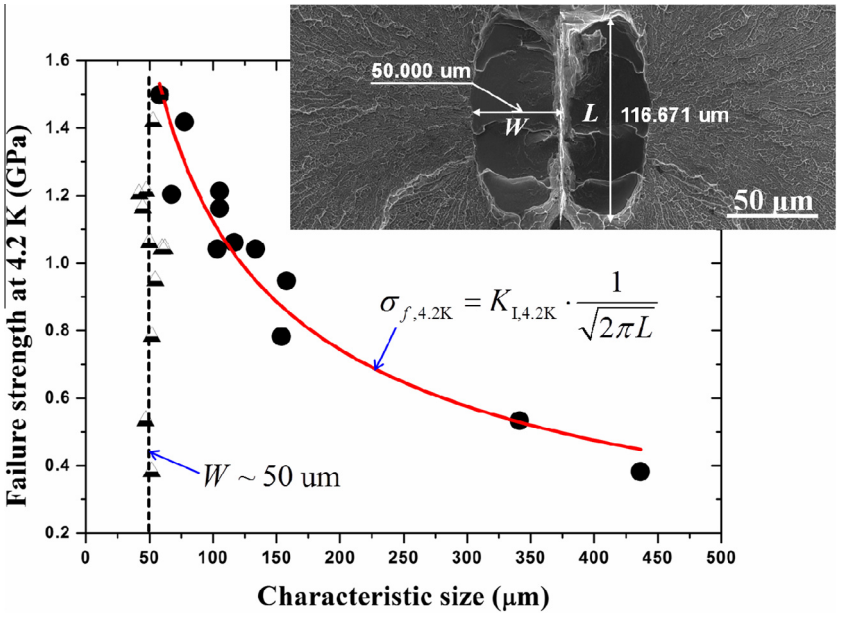

Fig. 6. Failure strength $\sigma_{f,4.2K}$ at 4.2 K as a function of the characteristic width W and length L of crack nucleation regions, indicating a scaling law between $\sigma_{f,4.2K}$ and L that is described well by Eq. (1). The inset shows a matched crack nucleation region with $W \approx 50$ μm and $L \approx 117$ μm.

1 [47] or brittle metallic glass systems (Mg- or Fe-based) [14,16,19]. Such low toughness guarantees the brittle propagation of cracks via the cavitation mechanism, which is verified by the dimples and nanoscale periodic corrugations observed in the propagation region (Fig. 5).

4. Discussion

The above experimental observations allow us to obtain two basic pieces of information. The first is that, with decreasing temperature from 300 to 4.2 K, Vitreloy 1 shows an obvious transition from shear- to tension-dominated failure, demonstrating a low-temperature-enhanced normal stress sensitivity. The second is that the tensile failure is mediated by the cavitation process ahead of crack tips. In the uniaxial stress state, the cavitation should originate from the significant dilatation induced by shear. Therefore, the inherent competition between shear and dilatation should be responsible for the temperature-dependent normal stress sensitivity of failure observed in the Vitreloy 1.

The Mohr–Coulomb criterion has been widely used to describe the normal stress effect of shear failure in metallic glasses [20,23,25,27], which can be expressed as

$$\tau_\theta + \alpha\sigma_\theta = \tau_0 \tag{2}$$

where τ_0 is the critical failure stress in pure shear, which should be temperature dependent [13,21,48], and τ_θ and σ_θ are the shear and normal stresses on the failure plane, respectively, and can be derived from

$$\tau_\theta = \sigma_f \sin(\theta)\cos(\theta) \tag{3}$$

$$\sigma_\theta = \sigma_f \sin^2(\theta) \tag{4}$$

For metallic glasses, the normal stress sensitivity coefficient α can be regarded as a dilatational factor that characterizes the relative ratio of shear to dilatation. A larger α implies an easier dilatation, with a relatively low critical normal stress $\sigma_0 = \tau_0/\alpha$. Macroscopically, the dilatational factor α can be directly related to the fracture angle θ under the uniaxial tension condition:

$$\alpha = -\frac{\cos(2\theta)}{\sin(2\theta)} \tag{5}$$

According to the measured fracture angle θ in Fig. 1b, the change of α with temperature is given in Fig. 7a. Note that α increases gradually with decreasing temperature. However, below the transition point (20 K), the value of α becomes significantly large. The critical transition value of α at 20 K is close to the suggested value ($\sqrt{1/2}$) that separates the shear-dominated failure from the tensile failure in metallic glasses [29,39].

Based on the measured failure strength σ_f (Fig. 1a) and fracture angle θ (Fig. 1b), as well as the calculated dilatational factor α (Fig. 7a), we can further calculate τ_θ, σ_θ, τ_0 and σ_0 at different temperatures, as shown in Fig. 7b (where the dashed lines are just guides for the eye). It can be seen that, with decreasing temperature, both τ_θ and σ_θ first increase gradually, indicating a low-temperature-induced strengthening. However, across the transition point (20 K), the value of τ_θ shows a significant drop, whereas σ_θ decreases only a little. More importantly, the temperature dependence of the critical stresses τ_0 and σ_0 exhibits very different trends. With decreasing temperature, the critical shear stress τ_0 increases gradually at $T > 20$ K, then increases remarkably below 20 K. However, the critical normal stress σ_0 continues to decrease down the whole temperature range. It is worth noting that σ_0 becomes

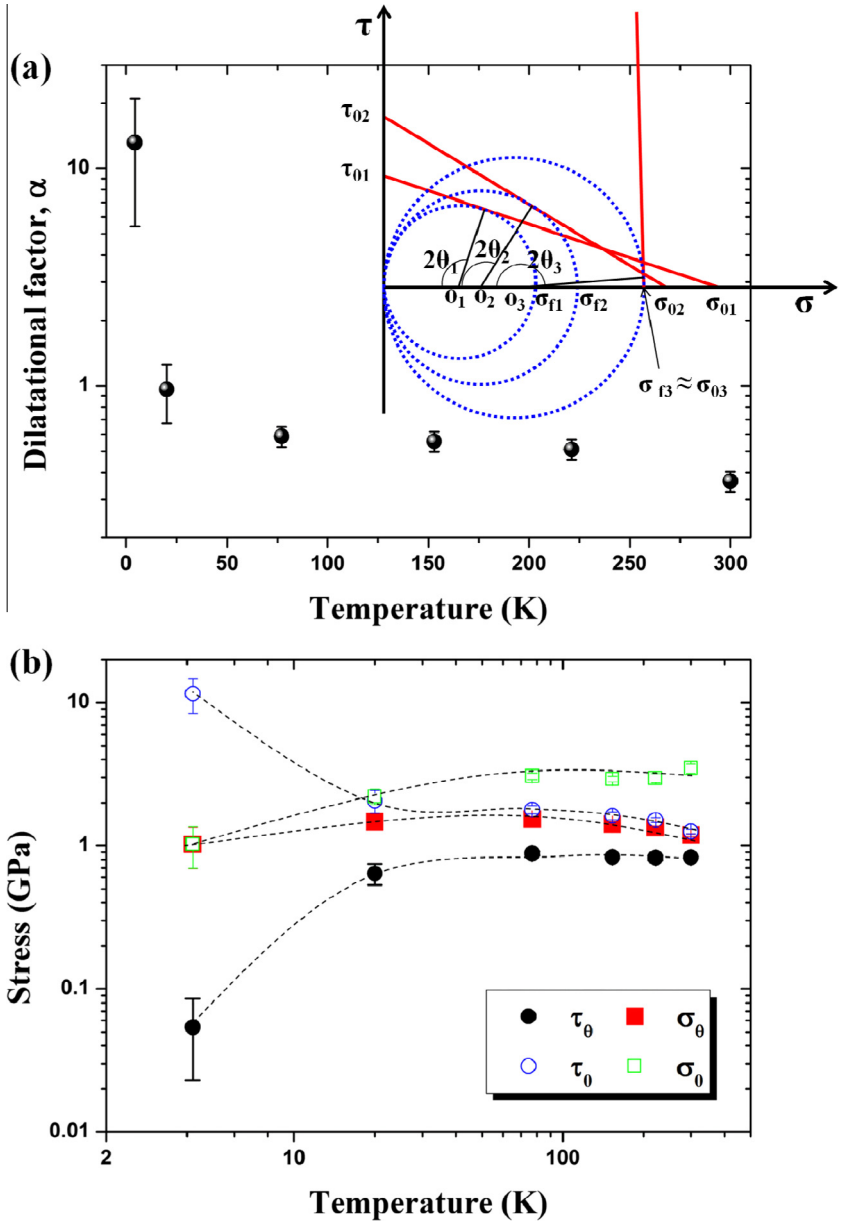

Fig. 7. (a) Variation of the dilatational factor calculated by Eq. (5) with decreasing temperature. (b) Variation of the shear and normal stresses on the failure plane, as well as the critical shear and normal stresses of the material with decreasing temperature. The inset in (a) illustrates the evolution of Mohr's circle and the failure line, i.e. Eq. (2), with temperature.

smaller than τ_0 below 20 K, which means that tensile failure occurs more easily than shear failure. At liquid helium temperature (4.2 K), σ_θ is almost equal to σ_0, but $\tau_\theta \ll \sigma_\theta$ and $\sigma_0 \ll \tau_0$, confirming the occurrence of tensile failure. It is clear that decreasing temperature enhances the critical shear stress τ_0 but reduces the critical normal stress σ_0 to induce the shear-to-tension transition of failure of metallic glasses. Recently, Murali et al. [1] performed a simulation of the fracture behavior of both ductile CuZr and brittle FeP metallic glasses. They found that in the CuZr glass, where shear failure dominates, the critical cavitation stress is higher than in the FeP glass, the failure of which is dominated by cavitation, though the stress fluctuation is much greater in the latter than in the former. If we compare the critical cavitation stress with the critical normal stress σ_0 in the present work, it confirms that the change of σ_0 with temperature (Fig. 7b) is reasonable. The value of σ_0 in the dilatational failure case (4.2 K) is less than that in the temperature range where the failure is shear dominated, but the fluctuation of σ_0 at 4.2 K is much more significant.

The results revealed in Figs. 1 and 7 can be illustrated in a σ–τ coordinate by examining the failure line and the Mohr's circle, as indicated by the red[1] solid lines and blue dashed circles, respectively, in the inset of Fig. 1a. Let us assume that, at room temperature, the Mohr–Coulomb

[1] For interpretation of color in Fig. 7, the reader is referred to the web version of this article.

criterion, i.e. Eq. (2), corresponds to the failure line $\tau_{01}\sigma_{01}$ with the slope α_1; the Mohr's circle o_1 represents the distribution of the stress state (τ, σ) at any plane in the specimen. When the Mohr's circle o_1 touches the failure line $\tau_{01}\sigma_{01}$, the specimen fails, with the failure stress σ_{f1} along the failure plane at the fracture angle θ_1. If σ_{01} is very large relative to τ_{01}, that is, $\alpha_1 \to 0$, the failure should be pure shear, with $\theta_1 \to 45°$. In this case, the Mohr–Coulomb criterion actually simplifies to the Tresca criterion. For the present Vitreloy 1, $\alpha_1 \neq 0$, and this leads to a fracture angle larger than 45°, though the failure is still triggered by shear stress. When the temperature decreases, τ_{01} increases to τ_{02} but σ_{01} decreases to σ_{02} and thus α_1 increases to α_2, as revealed in Fig. 7. This corresponds to the change in the failure line from $\tau_{01}\sigma_{01}$ to $\tau_{02}\sigma_{02}$, and the Mohr's circle moves from o_1 to o_2. The fracture angle θ_2, the failure strength σ_{f2} and its stress components $(\tau_{\theta_2}, \sigma_{\theta_2})$ on the failure plane also increase, which is consistent with the experimental observations (see Figs. 1a and 7b). After the temperature decreases across the transition point (20 K), τ_{03} becomes much greater than σ_{03}, thus α_3 is significantly large, e.g. at 4.2 K. In this case, the failure line $\tau_{03}\sigma_{03}$ is approximately perpendicular to the σ axis, and the failure point approaches the point (0, σ_{03}). The fracture angle becomes very close to 90° (see Fig. 1b); the normal stress σ_{θ_3} on the failure plane should approach the failure strength σ_{f3}, which is nearly equal to the critical normal stress σ_{03}, while the shear stress τ_{θ_3} becomes negligibly small.

The low-temperature-enhanced normal stress sensitivity of macroscopic failure can be further understood in the microscopic picture: the shear-to-dilatation transition of STZs. At room temperature, the STZ is shear dominated, accompanied by a slight dilatation. The operation of one STZ gives rise, in the surrounding elastic medium, to an "Eshelby"-like localized shear distortion [10], and triggers an avalanche-like behavior of neighboring STZs to form shear bands [49–52], leading to a macroscopic shear-dominated failure. With decreasing temperature, the activation of an STZ needs to surmount a higher energy barrier and thus requires a higher activation stress in order to occur. This is why the critical shear stress τ_0 (Fig. 7b) and the failure strength σ_f (Fig. 1a) of materials increases at lower temperatures, showing the strengthening behavior at $T > 20$ K. On the other hand, the increase in the critical shear stress will in turn improve the dilatation ability of STZs, since the STZ has the nature of shear thinning or -dilatation due to the disordered structure. This picture is supported by the common observation that metallic glasses with higher strengths are always accompanied by a more significant softening to cracking [53–54]. Therefore, the STZ at lower temperatures becomes more inclined to dilatation operations, macroscopically corresponding to the decrease in the critical normal tensile stress σ_0 (Fig. 7b). Nevertheless, at temperatures that are not low enough, the shear operation of STZ still predominates in the competition with its induced dilatation. This is confirmed by the result that the critical shear stress τ_0 is much less than the critical normal tensile stress σ_0 at $T > 20$ K (Fig. 7b). With further decreasing temperature, the shear operations of STZ become increasingly difficult, whereas, in contrast, the dilatation operations become easier. The former corresponds to the increase in τ_0 and the latter to the decrease in σ_0. The STZ will eventually be dominated by dilatation below a critical temperature (here about 20 K), which is indicated as $\sigma_0 < \tau_0$ at $T < 20$ K (Fig. 7b). In fact, so long as $\sigma_0 \leqslant \sqrt{2\tau_0}$, dilatation-dominated tensile failure will occur [29,39]. That means that the real critical temperature will be slightly higher than 20 K. Once the STZ behaves in a dilatation-dominated fashion [14], the softening (or weakening) process will govern the strength of the material, corresponding to the decrease in macroscopic failure strength observed at $T < 20$ K (Fig. 1a). Therefore, the failure of metallic glasses at low temperatures is determined by the competition between the low-temperature-induced shear strengthening and the resulting dilatational softening. Moreover, Fig. 7b demonstrates that it is very hard to shear a dilatation-mode STZ due to its extremely high critical shear stress. We find that the value of τ_0 at 4.2 K is comparable to the maximum shear strength (8.73 GPa) of Vitreloy 1 theoretically predicted by Wang and Li [55].

5. Conclusions

Under quasi-static uniaxial tensions, we achieved the transition from shear- to dilatational failure of a typical tough Zr-based bulk metallic glass by cryogenically cooling it from 300 K down to 4.2 K. Our primary finding is that the normal stress (or pressure) sensitivity of failure of metallic glasses is temperature dependent and becomes more significant with decreasing temperature. Macroscopically, this failure behavior can be described well by the Mohr–Coulomb criterion by considering a temperature-dependent dilatational factor or the ratio of the critical shear stress to the critical normal stress of the material. Microscopically, the low-temperature-enhanced normal stress sensitivity of failure implies that the relative contribution of shear to the dilatation of STZs determines the macroscopic failure of metallic glasses. This physical picture is consistent with the well-known Poisson's ratio criterion for plasticity of amorphous solids [30,56,57]. Our work substantiates the idea that stress-driven STZs need thermal assistance, and further predicts that a thermal or very-low-temperature STZs are prone to suffer a dilatation mode [14] due to their relatively low critical stress.

Acknowledgements

The authors are very grateful to Konrad Samwer for enlightening discussion and H.M. Xiao, Z. Ling and G.H. Duan for technical assistance. This work was supported by the National Nature Science Foundation of China (Grant Nos. 11372315, 11132011, 11023001 and 51171138). M.Q.J. acknowledges the Alexander von Humboldt Foundation for support with a post-doctoral

fellowship. We are very grateful to two anonymous reviewers for their helpful comments, which have improved our manuscript significantly.

References

[1] Murali P, Guo TF, Zhang YW, Narasimhan R, Li Y, Gao HJ. Phys Rev Lett 2011;107:215501.
[2] Ye JC, Lu J, Liu CT, Wang Q, Yang Y. Nat Mater 2011;9:619.
[3] Guan P, Lu S, Spector MJB, Valavala PK, Falk ML. Phys Rev Lett 2013;110:185502.
[4] Chattoraj J, Lemaître A. Phys Rev Lett 2013;111:066001.
[5] Li L, Homer ER, Schuh CA. Acta Mater 2013;61:3347.
[6] Miracle DB. Nat Mater 2004;3:697.
[7] Sheng HW, Luo WK, Alamgir FM, Bai JM, Ma E. Nature 2006;439:419.
[8] Ma D, Stoica AD, Wang X-L. Nat Mater 2009;8:30.
[9] Hirata A, Guan PF, Fujita T, Hirotsu Y, Inoue A, Yavari AR, et al. Nat Mater 2011;10:28.
[10] Argon AS. Acta Metall 1979;27:47.
[11] Falk ML, Langer JS. Phys Rev E 1998;57:7192.
[12] Homer ER, Schuh CA. Acta Mater 2009;57:2823.
[13] Schuh CA, Hufnagel TC, Ramamurty U. Acta Mater 2007;55:4067.
[14] Jiang MQ, Ling Z, Meng JX, Dai LH. Philos Mag 2008;88:407.
[15] Jiang MQ, Dai LH. Acta Mater 2011;59:4525.
[16] Wang G, Zhao DQ, Bai HY, Pan MX, Xia AL, Han BS, et al. Phys Rev Lett 2007;98:235501.
[17] Bouchaud E, Boivin D, Pouchou JL, Bonamy D, Poon B, Ravichandran G. Europhys Lett 2008;83:66006.
[18] Huang X, Ling Z, Zhang HS, Ma J, Dai LH. J Appl Phys 2011;110:103519.
[19] Xi XK, Zhao DQ, Pan MX, Wang WH, Wu Y, Lewandowski JJ. Phys Rev Lett 2005;94:125501.
[20] Schuh CA, Lund AC. Nat Mater 2003;2:449.
[21] Sun L, Jiang MQ, Dai LH. Scr Mater 2010;63:943.
[22] Lowhaphandu P, Montgomery SL, Lewandowski JJ. Scr Mater 1999;41:19.
[23] Zhang ZF, Echert J, Schultz L. Acta Mater 2003;51:1167.
[24] Yuan FP, Prakash V, Lewandowski JJ. Mech Mater 2010;42:248.
[25] Caris J, Lewandowski JJ. Acta Mater 2009;58:1026.
[26] Lewandowski JJ, Lowhaphandu P. Philos Mag A 2002;82:3427.
[27] Lund AC, Schuh CA. Acta Mater 2003;51:5399.
[28] Yu GS, Lin JG, Mo M, Wang XF, Wang FH, Wen CE. Mater Sci Eng A 2007;460–461:58.
[29] Chen Y, Jiang MQ, Wei XJ, Dai LH. Philos Mag 2011;91:4536.
[30] Lewandowski JJ, Wang WH, Greer AL. Philos Mag Lett 2005;85:77.
[31] Johnson WL. MRS Bull 1999;24:42.
[32] Li HQ, Fan G, Tao KX, Choo H, Liaw PK. Adv Mater 2006;18:752.
[33] Keryvin V, Prasad KE, Gueguen Y, Sangleboeuf JC, Ramamurty U. Philos Mag 2008;88:1773.
[34] Kawashima A, Yokoyama Y, Seki I, Kurishita H, Fukuhara M, Kimura H, et al. Mater Trans 2009;50:2685.
[35] Dubach A, Dalla Torre FH, Loffler JF. Acta Mater 2009;57:881.
[36] Anderson TL. Fracture mechanics: fundamentals and applications. 3rd ed. London: Taylor & Francis Group; 2005.
[37] Wu T-W, Spaepen F. Philos Mag B 1990;61:739.
[38] Zhang ZF, He G, Eckert J, Schultz L. Phys Rev Lett 2003;91:045505.
[39] Zhang ZF, Eckert J. Phys Rev Lett 2005;94:094301.
[40] Saffman PG, Taylor G. Proc R Soc Lond A 1958;245:312.
[41] Argon AS, Salama MS. Mater Sci Eng 1976;23:219.
[42] Leamy HJ, Chen HS, Wang TT. Metall Trans A 1972;3:699.
[43] Pampillo CA. J Mater Sci 1975;10:1194.
[44] Qu RT, Stoica M, Eckert J, Zhang ZF. J Appl Phys 2010;108:063509.
[45] Meng JX, Ling Z, Jiang MQ, Zhang HS, Dai LH. Appl Phys Lett 2008;92:171909.
[46] Jiang MQ, Meng JX, Gao JB, Wang XL, Rouxel T, Keryvin V, et al. Intermetallics 2010;18:2468.
[47] Raghavan R, Murali P, Ramamurty U. Acta Mater 2009;57:3332.
[48] Johnson WL, Samwer K. Phys Rev Lett 2005;95:195501.
[49] Lemaître A, Caroli C. Phys Rev Lett 2009;103:065501.
[50] Argon AS. Philos Mag 2013;93:3795.
[51] Jiao W, Sun BA, Wen P, Bai HY, Kong QP, Wang WH. Appl Phys Lett 2013;103:081904.
[52] Antonaglia J, Wright WJ, Gu XJ, Byer RR, Hufnagel TC, LeBlanc M, et al. Phys Rev Lett 2014;112:155501.
[53] Lu J, Ravichandran G, Johnson WL. Acta Mater 2003;51:3429.
[54] Zhang M, Liu L, Wu Y. J Chem Phys 2013;139:164508.
[55] Wang H, Li M. Phys Rev Lett 2013;111:065507.
[56] Jiang MQ, Dai LH. Philos Mag Lett 2010;90:269.
[57] Greaves GN, Greer AL, Lakes RS, Rouxel T. Nat Mater 2011;10:823.